

## An Observing System Simulation Experiment for the Indian Ocean

GABRIEL A. VECCHI\* AND MATTHEW J. HARRISON

*NOAA/Geophysical Fluid Dynamics Laboratory, Princeton, New Jersey*

(Manuscript received 2 May 2005, in final form 9 September 2005)

### ABSTRACT

An integrated in situ Indian Ocean observing system (IndOOS) is simulated using a high-resolution ocean general circulation model (OGCM) with daily mean forcing, including an estimate of subdaily oceanic variability derived from observations. The inclusion of subdaily noise is fundamental to the results; in the mixed layer it is parameterized as Gaussian noise with an rms of  $0.1^{\circ}\text{C}$ ; below the mixed layer a Gaussian interface displacement with an rms of 7 m is used. The focus of this assessment is on the ability of an IndOOS—comprising a  $3^{\circ} \times 3^{\circ}$  Argo profiling float array, a series of frequently repeated XBT lines, and an array of moored buoys—to observe the interannual and subseasonal variability of subsurface Indian Ocean temperature. The simulated IndOOS captures much of the OGCM interannual subsurface temperature variability.

A fully deployed Argo array with 10-day sampling interval is able to capture a significant part of the Indian Ocean interannual temperature variability; a 5-day sampling interval degrades its ability to capture variability. The proposed moored buoy array and frequently repeated XBT lines provide complementary information in key regions, particularly the Java/Sumatra and Somali upwelling and equatorial regions. Since the subdaily noise is of the same order as the subseasonal signal and since much of the variability is submonthly, a 5-day sampling interval does not drastically enhance the ability of Argo to capture the OGCM subseasonal variability. However, as sampling intervals are decreased, there is enhanced divergence of the Argo floats, diminished ability to quality control data, and a decreased lifetime of the floats; these factors argue against attempting to resolve subseasonal variability with Argo by shortening the sampling interval. A moored array is essential to capturing the subseasonal and near-equatorial variability in the model, and the proposed moored buoy locations span the region of strong subseasonal variability. On the whole, the proposed IndOOS significantly enhances the ability to capture both interannual and subseasonal variability in the Indian Ocean.

### 1. Introduction

The Indian Ocean exhibits energetic variability on many time and space scales. There is significant interest in observing, understanding, and predicting this variability (e.g., this special issue). In recent years the first steps toward implementing a sustained, integrated Indian Ocean observing system (IndOOS) have been taken: for example, Argo profiling floats continue to be deployed in the Indian Ocean by researchers from various nations, moored buoys have been placed at various locations in the Indian basin (e.g., Premkumar et al.

2000; Bhat et al. 2001; Masumoto et al. 2005a), and efforts are under way to coordinate a basinwide, multisensor observing system (e.g., Meyers et al. 2000; Masumoto et al. 2005b; CLIVAR–GOOS Indian Ocean Panel 2006). To help in the process of the observing system development, various groups have undertaken observing system simulation experiments (OSSEs) using diverse methods and models (e.g., Schiller et al. 2004; Oke and Schiller 2007; Ballabrera-Poy et al. 2007; T. Lee 2005, personal communication), prior to the full deployment of the observing system. This paper describes the methods and results of one such OSSE.

The Indian Ocean region exhibits large-scale atmospheric and oceanic variability on a variety of time scales, including subseasonal, seasonal, and interannual; there have also been pronounced changes to Indian Ocean oceanic conditions over recent decades (e.g., Boyer et al. 2005; Levitus et al. 2005). See Schott and McCreary (2001), Annamalai and Murtugudde (2004), and Yamagata et al. (2004) for reviews of Indian

---

\* UCAR Visiting Scientist Program, Boulder, Colorado.

---

*Corresponding author address:* Dr. Gabriel A. Vecchi, NOAA/Geophysical Fluid Dynamics Laboratory, Princeton Forrestal Campus, Rte. 1, P.O. Box 308, Princeton, NJ 08542-0308.  
E-mail: gabriel.a.vecchi@noaa.gov

Ocean variability. Characterizing and understanding interannual variability in the Indian Ocean, its relationship to global ocean–atmosphere variability, and its relationship to weather and climate variability over land is a topic of significant interest (e.g., Ju and Slingo 1995; Nicholls 1995; Harrison and Larkin 1998; Webster et al. 1998; Saji et al. 1999; Webster et al. 1999; Loshnigg and Webster 2000; Larkin and Harrison 2001; Schott and McCreary 2001; Lau and Nath 2003; Annamalai and Murtugudde 2004; Yamagata et al. 2004; Vecchi and Harrison 2004; Song et al. 2007).

The Indian Ocean ocean–atmosphere subseasonal variability occurs on many time scales and is evident in many regions of the Indian Ocean.<sup>1</sup> For example, in situ and satellite observations have found strong intraseasonal sea surface temperature (SST) swings associated with the southwest monsoon’s northward propagating intraseasonal oscillation in the Bay of Bengal (Premkumar et al. 2000; Bhat et al. 2001; Sengupta and Ravichandran 2001; Webster et al. 2002; Vecchi and Harrison 2002; Wang et al. 2005). There is substantial subseasonal SST variability [ $O(1^{\circ}\text{--}2^{\circ}\text{C})$ ] in the southern Indian Ocean thermocline ridge, a region between  $8^{\circ}$  and  $3^{\circ}\text{S}$  in which the thermocline is close to the surface through surface divergence induced by the strong wind stress curl (Harrison and Vecchi 2001; Duvel et al. 2004). Model and observational studies have found that the equatorial Indian Ocean has strong intraseasonal oceanic variability on a variety of time scales (e.g., Sengupta et al. 2004; Masumoto et al. 2005a). In the western Arabian Sea there is substantial variability to oceanic frontal features, with evidence of significant feedbacks to the atmosphere (Vecchi et al. 2004).

To date satellites have been the only platform for observing the basinwide subseasonal oceanic variability; thus, a lack of subsurface observations has obscured our understanding of the mechanisms behind them; the depth over which they occur, the circulation changes associated with them, etc. all remain not fully understood. In addition, the satellite representation of the subseasonal SST variability may be incomplete (e.g., Bhat et al. 2004). The full character and climate significance of the subseasonal oceanic variability is not yet fully understood, but recent results suggest that it may be of significant impact. For example, intermediate

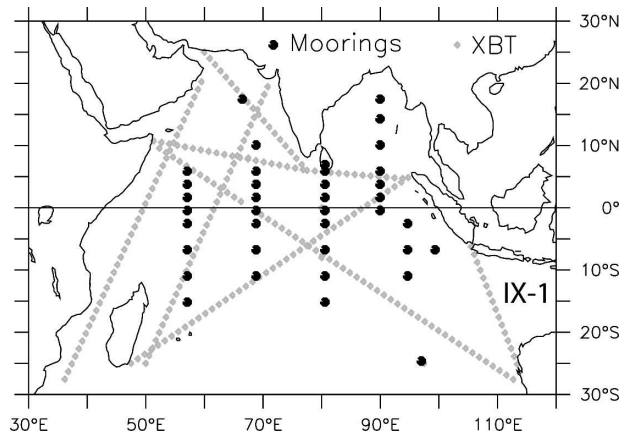


FIG. 1. An IndOOS comprising Argo floats, XBT lines, and moored buoys. Other elements of an observing system will include satellites, drifting buoys, carbon lines, etc., which are not addressed in this paper. Adapted from CLIVAR–GOOS Indian Ocean Panel (2006).

coupled model analyses suggest that the Bay of Bengal SST changes may be dynamically important to the evolution of the northward propagating “intraseasonal oscillation” (ISO; Fu et al. 2003)—a feature of significant social and economic impact in the region. Coupled model results suggest that intraseasonal convective events could play a role in inhibiting the development of “Indian Ocean Dipole–Zonal Mode” events (e.g., Gualdi et al. 2003; Song et al. 2007). Further, the thermocline ridge SST swings are associated with the Madden–Julian oscillation (e.g., Madden and Julian 1994), which originates in the Indian Ocean region and connects to weather variability around the globe (e.g., Mo and Higgins 1998; Maloney and Hartmann 2000; Bond and Vecchi 2003; Vecchi and Bond 2004). At the very least, the intensity and ubiquity of the subseasonal variability presents a background upon which observations of longer-than-seasonal variability need to be understood, and its aliasing should be avoided.

An integrated in situ observing system has been proposed for the Indian Ocean, comprising—among other platforms—an Argo drifting buoy array, frequently repeated XBT lines, and a moored buoy array (Fig. 1: CLIVAR–GOOS Indian Ocean Panel 2006). In this paper we present an assessment of a proposed integrated, multiplatform observing system, and examine the extent to which the observing system is able to represent large-scale subseasonal and interannual variability of subsurface temperature. In the next section we describe the model used in these OSSEs. Section 3 describes the technique used to perform the OSSEs: particular interest is placed on developing a parameterization of sub-daily temperature variability (section 3c). Section 4 ex-

<sup>1</sup> Note that throughout this paper we have defined subseasonal variability to be that with time scales between 61 and 3 days, intraseasonal variability is the subset of subseasonal variability greater than 30 days, and submonthly variability is the subset of subseasonal variability with time scales less than 30 days.

plores the ability of the evaluated Indian Ocean observing system to capture interannual and subseasonal variability. Finally, Section 5 offers a summary and discussion of the results.

## 2. Model

### a. Description

We use the National Oceanic and Atmospheric Administration/Geophysical Fluid Dynamics Laboratory (NOAA/GFDL) primitive equation OGCM, the Modular Ocean Model version 2 (MOM2), in an Indian Ocean basin configuration. The configuration is similar to that used previously in studies of the tropical Pacific (e.g., Vecchi and Harrison 2003, 2005). The model domain is 30°S–30°N, 30°–117°E, and is represented on an Arakawa B grid with a variable zonal resolution starting at  $\frac{1}{3}^\circ$  from the western boundary of the basin until 55°E, increasing to  $\frac{1}{2}^\circ$  by 95°E; the meridional resolution is  $\frac{1}{3}^\circ$  from 15°S to 25°N, increasing to 2.5° at the southern boundary and 1.5° at the northern boundary. The model has 27 levels in the vertical, with 10 in the upper 100 m; the model time step is 1 h. Vertical mixing is parameterized using the Richardson number-dependent scheme of Pacanowski and Philander (1981) with parameters as in Vecchi and Harrison (2003, 2005). Horizontal mixing is parameterized as eddy diffusion, with eddy viscosity coefficient  $A_v$  of  $1 \times 10^3 \text{ m}^2 \text{ s}^{-1}$ , and heat diffusion coefficient  $A_h$  of  $2 \times 10^3 \text{ m}^2 \text{ s}^{-1}$ . The model does not have a representation for the Indonesian Throughflow, and there is no flow through the straits of the Indonesian Archipelago; at the southern boundary (30°S) a 5°-latitude-wide sponge restores temperature and salinity back to the Levitus (1982) climatology with a 30-day time scale. To initialize the model hindcast, the OGCM was spun up for 10 years using the monthly mean climatological wind stress field of Harrison (1989), with fluxes parameterized as in Vecchi and Harrison (2003, 2005). For all experiments, sea surface salinity was restored to the annual mean Levitus (1982) climatology using a 50-day restoring time scale.

Two model hindcast experiments were run starting from the end of this 10-yr spin up with climatology: one using the 1986–2003 wind forcing computed from the European Centre for Medium-Range Weather Forecasts (ECMWF 1989) 12-hourly,  $2.5^\circ \times 2.5^\circ$  resolution operational 10-m wind analysis and another using 2000–02 wind data from the National Aeronautics and Space Administration (NASA) Quick Scatterometer (QuikSCAT), made available by NASA's Jet Propulsion Laboratory (JPL). Microwave scatterometry gives us

the ability to explore basin-scale modes of vector wind variability in an unprecedented manner. We use NASA/JPL's QuikSCAT level-3 satellite vector wind product, with each vector component (zonal and meridional) and wind speed for both ascending and descending tracks gridded on a daily,  $0.25^\circ \times 0.25^\circ$  grid. A daily dataset for each component and for wind speed is generated by averaging the ascending and descending tracks (when both overlap on the same day) or by using the track that is present that day. Filled datasets for each wind component and wind speed are then generated by linear interpolation in time (gaps are generally less than 4 days long).

For both hindcast experiments surface momentum fluxes are parameterized using the "bulk formulae" of Large and Pond (1981), and the surface latent and sensible heat fluxes are parameterized using the "bulk formulae" of Large and Pond (1982). For the bulk formulas, wind velocities are adjusted to velocities relative to the ocean surface velocity by subtracting the vector velocity of the upper-ocean model grid cell; sea surface temperature is taken to be the temperature at the upper-ocean grid cell, the daily mean air temperature is taken from the National Centers for Environmental Prediction–National Center for Atmospheric Research (NCEP–NCAR) Reanalysis-2; relative humidity is assumed constant at 85%. Radiative forcing at the surface of the ocean is taken from the daily mean values of the NCEP–NCAR Reanalysis-2 product; incoming solar radiation is distributed in the vertical using a double exponential with 40% of the energy flux absorbed with a 2-m *e*-folding scale, and 60% absorbed with a 35-m *e*-folding scale.

Figure 2 compares climatological SST and surface currents for two seasons, the southwest and northeast monsoons, from the 1986–2003 ECMWF-forced hindcast with those from the SST climatology computed from the NCEP weekly  $1^\circ \times 1^\circ$  SST optimal interpolation (OI) version 2 (Reynolds and Smith 1994; Reynolds et al. 2002) and from a monthly climatology derived from the long-term ship-drift records of Richardson and McKee (1989). The Richardson and McKee data compare well with the surface climatology of Mariano et al. (1995), though the Mariano et al. currents tend to be slightly stronger. The model represents the seasonal changes in the surface currents relatively well, including the reversal of the western boundary current, the equatorial current changes, and the mean currents in the southern Indian Ocean. There are regional differences between the model and observations (in particular, in the region of the Indonesian Throughflow, which is not represented in the model), but, on the whole, the model

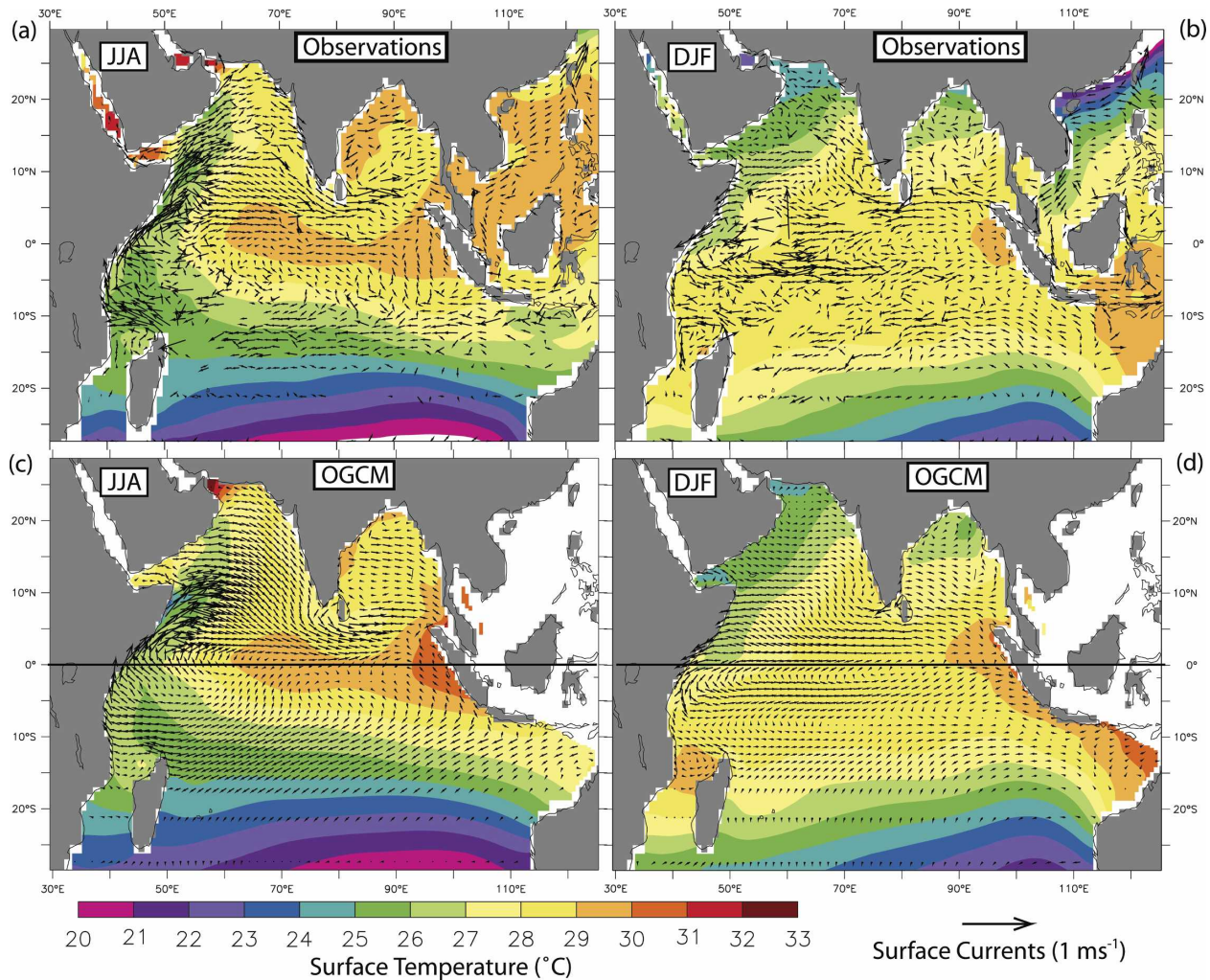


FIG. 2. Climatological-mean SST and surface current ( $u, v$ ) data for (a) OGCM and (c) observations in December–January and (b) OGCM and (d) observations in June–July. Observational SST climatology computed from the 1982–2003 NOAA SST OI version 2 analysis (Reynolds et al. 2002); surface currents taken from the ship-drift climatology (Richardson and McKee 1989). OGCM climatology computed from the 1986–2002 ECMWF wind-forced experiment. SST shaded in units of  $^{\circ}\text{C}$ ; currents shown as vectors with scale vector  $1 \text{ m s}^{-1}$ .

reproduces the principal features of the observed seasonal variability of SST and surface currents.

### b. Model variance

A principal focus of this analysis is the impact of submonthly variability on measurements of greater than monthly subsurface temperature variations and the ability of the observing system to resolve the energetic subseasonal variability in the Indian Ocean; in this section we detail the regions of strong submonthly temperature variability in the OGCM. The model output was saved as daily averages and there is no diurnal or tidal forcing in the model, so we confine our analysis in this section to time scales between 2 days and 1 month. A parameterization for the subdaily variability is devel-

oped from moored observations, and is described in section 3c.

A prominent feature of the subseasonal variability of SST is strong temperature variations along the thermocline ridge centered between  $10^{\circ}$  and  $3^{\circ}\text{S}$  during boreal winter/spring (Harrison and Vecchi 2001; Duvel et al. 2004), which were first identified using SST data from the Tropical Rainfall Measuring Mission (TRMM) Microwave Imager (TMI; Kummerow et al. 2000). The thermocline ridge subseasonal temperature variation events are evident in the OGCM experiments forced both with QuikSCAT and ECMWF winds, though their amplitudes are around half that seen in TMI (not shown). The amplitude of the variability is slightly larger in the QuikSCAT-forced run than in the ECMWF run. The weak SST variability with respect to satellite

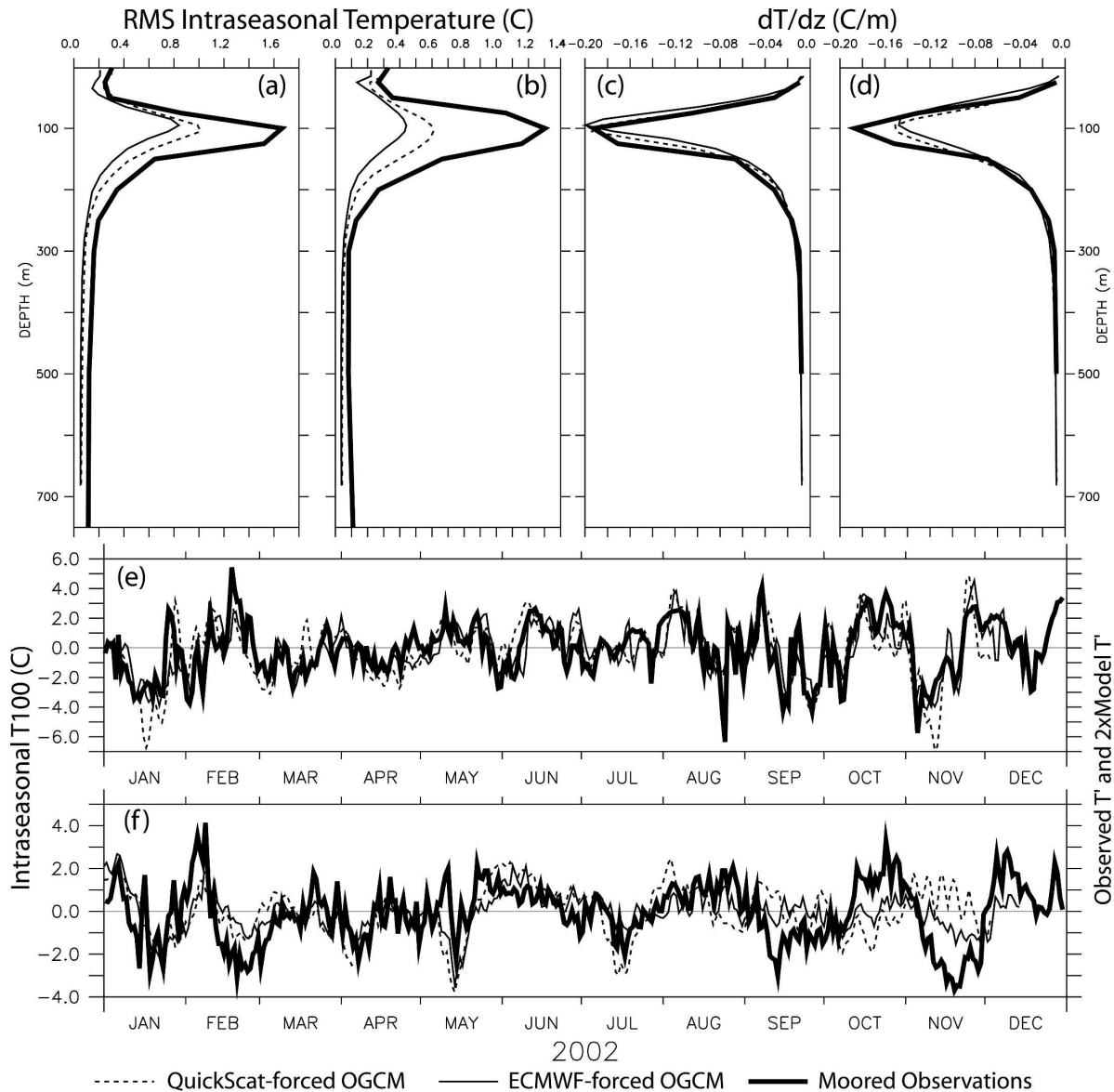


FIG. 3. Standard deviation of subseasonal (<61 day) temperature variability at (a)  $1.5^{\circ}\text{S}$ ,  $90^{\circ}\text{E}$  and (b)  $5^{\circ}\text{S}$ ,  $95^{\circ}\text{E}$ , units:  $^{\circ}\text{C}$ . Vertical gradient of temperature at (c)  $1.5^{\circ}\text{S}$ ,  $90^{\circ}\text{E}$  and (d)  $5^{\circ}\text{S}$ ,  $95^{\circ}\text{E}$ , units:  $^{\circ}\text{C m}^{-1}$ . (e),(f) Time series of subseasonal (<61 day) 100-m temperatures from the Indian Ocean TRITON moorings and  $2\times$  the subseasonal 100-m temperatures from the OGCM, units:  $^{\circ}\text{C}$ . Dark lines show values from the Indian Ocean TRITON moorings, light solid lines show values from ECMWF-forced run, and light dashed lines show values from the QuikSCAT-forced run.

observations could be due to a variety of factors, both model and forcing deficiencies. Nonetheless, the character and timing of the thermocline ridge cooling is well represented in the OGCM.

The two Triangle Trans-Ocean Buoy Network (TRITON) moorings that have been deployed at ( $1.5^{\circ}\text{S}$ ,  $90^{\circ}\text{E}$ ) and ( $5^{\circ}\text{S}$ ,  $95^{\circ}\text{E}$ ) since late 2001 allow us to evaluate the subseasonal variability of subsurface temperatures simulated by the models. Figures 3a and 3b show the standard deviations of modeled and observed

subseasonal (defined as daily minus 61-day centered running mean) temperature at the two TRITON mooring locations, for the year 2002. The location of the maximum variance is well represented by the OGCM with both forcing datasets; however, the modeled subseasonal temperature variability is only about half of that observed. It appears that the deficiency in the model is not coming principally from a too diffuse thermocline (a common feature of  $z$ -coordinate models) since the mean vertical temperature gradients in the

model compare well with those in observations (Figs. 3c and 3d). However, if the amplitude of the OGCM subseasonal temperature variations is doubled, there is a general agreement in the character and amplitude of the subseasonal variability at these locations; Figs. 3e and 3f show the time series of observed subseasonal 100-m temperature and twice the OGCM subseasonal 100-m temperature at the two TRITON mooring locations.

The recent moored ADCP data from Masumoto et al. (2005a) provide another opportunity to evaluate the model representation of subseasonal oceanic variability. Figure 4 shows the evolution of subseasonal currents in the eastern equatorial Indian Ocean through a reproduction of Fig. 2 from Masumoto et al. (2005a) in the center column along with equivalent figures from the two OGCM experiments on either side. Both models represent the basic character of the seasonal and subseasonal variability of subsurface currents; however, consistent with the model underestimate of subsurface temperature variability, the modeled subseasonal current variability appears weaker than that in observations. Interestingly, though the deep subsurface currents resulting from both wind-forcing datasets are comparable, the near-surface currents (including those outside the scope of the upward-looking ADCP) differ considerably.

We note that, as there are only two TRITON buoys available in the Indian Ocean region, the model validation is limited to these two buoy datasets. It is expected that, as the Indian Ocean Observing System comes on line, we will learn more from the added buoy subsurface temperature data that would be available and the model can be validated on a regional basis like the north Indian Ocean (Arabian Sea and Bay of Bengal, equatorial Indian Ocean, south Indian Ocean, etc.). In addition, the model underestimate of subseasonal current and subsurface temperature variability underscores the importance and necessity of an Indian Ocean observing system, which can resolve aspects of subseasonal variability. Until the data from the two TRITON moorings became available, we were not even aware that the temperature and current variability was weak: now we must strive to understand and correct the mechanisms that may be responsible for this underestimate. To do this, collocated observations of ocean thermal and current structure will be quite valuable.

Because of the evident underestimate of the amplitude of the subseasonal variability by the OGCM, we performed the OSSE experiments on two temperature datasets: 1) the original OGCM daily temperature data and 2) an “enhanced subseasonal” dataset in which the amplitude of the subseasonal temperature variability (as defined above) is doubled, but the 61-day smoothed

temperature is kept the same. Through the rest of the paper we will focus on the results from “enhanced OGCM” temperature data. Though the enhancement of the subseasonal temperature variability is an ad hoc correction, we use it since its temperature variations match the amplitude and character of those in available observations. Representative temperature variability is necessary to assess the potential aliasing of subseasonal variability in observations of interannual variability. We note that the underestimate in variability also likely affects the amplitude of subseasonal currents in the OGCM; however, for the OSSE experiments we keep the subseasonal currents from the original OGCM integration.

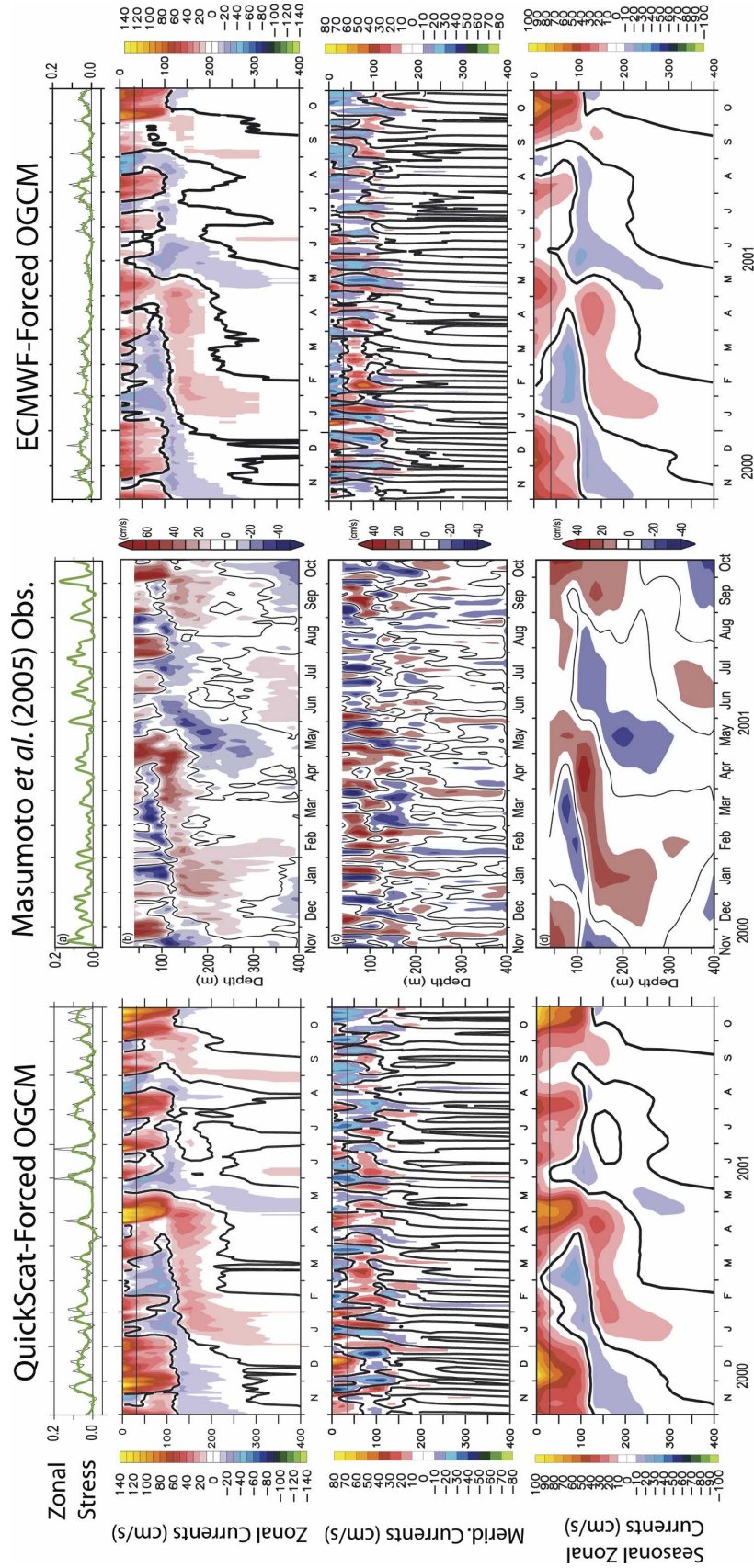
### 3. Techniques

#### a. *Subsampling strategy*

Throughout this analysis it is assumed that the failure rate of the observing system components is zero with the exception of Argo floats that are advected into shallow water (shallower than 1000 m). The instruments are also assumed to have no drift, random or systematic errors, or calibration problems; we make this assumption to study the impact of small-scale oceanic variations in isolation. We will consider the combined effectiveness of three components of the integrated observing system: the Argo profiling float array, the frequently repeated expendable bathythermograph (XBT) lines, and the proposed Indian Ocean moored buoy array.

#### 1) ARGO PROFILING FLOAT ARRAY

Argo floats are generally programmed to “sit” at 1000 dbar for 10 days before making an upward temperature and salinity profile from 2000 dbar and then sit at the surface between 8 and 14 h to telemeter the data to satellites before returning to 1000 m; in this configuration they have a nominal lifetime of around 3 years (e.g., Argo Science Team 2001). For the OSSEs, a fully deployed array of Argo floats is initially distributed uniformly over the Indian Ocean ( $3^\circ \times 3^\circ$  spacing), and is completely replaced every three years. This distribution represents an optimistic assumption since Argo floats are being deployed in a nonuniform manner in both space and time. However, we wish to explore a “best case scenario” of the fully deployed observing system. Further, since we do not know now at which time each region of the ocean will be seeded and since deployment of profiling floats is determined by many factors that are beyond our ability to model (ship availability,



funding, etc.), we have not endeavored to build more complicated algorithms, which we believe would likely give only the illusion of realism.

Except on their surfacing dates, each Argo float is advected by the model daily mean current at 1000 m, linearly interpolated to the location of the drifter; on the surfacing days the floats are advected for 10 h using the daily mean current at the upper grid box, and for 14 h using the current at 1000 m [though near the equator a longer surfacing time may be typical; S. Wijffels

(2005, personal communication)]. Each surfacing day an instantaneous profile of the temperature is taken. There are times when the simulated Argo floats are advected into regions in which the bathymetry is shallower than their resting depth of 1000 m. We deal with this situation by deactivating some of the floats that arrive at a location where the  $0^{\circ}20' \times 0^{\circ}20'$  bathymetry from Smith and Sandwell (1997) is shallower than 1000 m. Every day there is a probability ( $P_d$ ) that a float will be deactivated, given by

$$P_d = \begin{cases} 0, & \text{if } z > 1000 \text{ m} \\ 0.1(1000 \text{ m} - z)/900 \text{ m}, & \text{if } 1000 \text{ m} \geq z \geq 100 \text{ m} \\ 0.1, & \text{if } z > 100 \text{ m}, \end{cases}$$

where  $z$  is the bathymetric depth from the Smith and Sandwell (1997) data at each float location. After three years the floats are reinitialized at their original starting positions.

Because of the ubiquitous and strong subseasonal variability in the Indian Ocean, it has been suggested that Argo profiling floats in the tropical Indian Ocean region be programmed to sample only down to 1000 dbar and to have a sampling interval of 5 days rather than the standard 10 days. It has been suggested that the increased sampling rate would reduce aliasing of the subseasonal variability and, perhaps, even allow the subseasonal variability to be resolved by Argo (e.g., Schiller et al. 2004). The impact of 5-day sampling is explored by performing additional experiments with 5-day rather than 10-day sampling.

Figure 5 shows the location of the simulated Argo floats three years after their original regular grid “deployment” with the ECMWF- and QuikSCAT-forced OGCM experiments. The simulated floats show a divergence from regions of significant surface horizontal divergence: the southern tropical Indian Ocean thermocline ridge, the Java/Sumatra upwelling region, the Somali/Arabian upwelling zone, and the seasonal upwelling zone south of the Bay of Bengal [see Miyama et al. (2003) and Schott et al. (2004) for discussion of these upwelling zones]. These regions are of significant climate interest (e.g., Saji et al. 1999; Webster et al. 1999; Harrison and Vecchi 2001; Xie et al. 2002; Annamalai

and Murtugudde 2004; Schott et al. 2004; Vecchi and Harrison 2004; Yamagata et al. 2004), in part because the thermocline tends to be close to the surface. Ironically, the climate significance of these regions results from the very circulation that tends to remove the Argo floats. In spite of the loss to bottom topography and to the divergence from certain regions, the 10-day Argo profiling float array delivers significant coverage of the Indian Ocean. Note that the Argo floats with a 5-day sampling rate (Fig. 5) show a more prominent divergence/convergence, and more are lost due to shoaling and grounding in shallow waters. Most of the drift of the simulated Argo floats occurs during their residence at the surface where currents are significantly stronger and more variable than at 1000 m; when Argo floats surface twice as often, they drift twice as far. The degradation of the coverage of the Indian Ocean Argo array using a 5-day sampling is significant and should only be implemented if there are compelling benefits to doing so.

## 2) XBT LINES

The high spatial density and regular locations of ship tracks make XBTs a unique component of the global ocean observing system. In the Indian Ocean there have been a series of frequently repeated XBT lines that have been occupied with some regularity in decades—though some have not been occupied in recent

←

FIG. 4. Comparison of OGCM subsurface currents with those observed by the JAMSTEC upward-looking ADCP at  $0^{\circ}$ ,  $90^{\circ}$ E (Masumoto et al. 2005). (middle) Reproduction of Fig. 2 from Masumoto et al. (2005) showing from top to bottom the QuikSCAT weekly zonal wind stress (green time series), the ADCP-observed daily zonal currents, meridional currents, and monthly smoothed zonal currents. (left) As in the middle panels except for the OGCM forced by daily QuikSCAT winds; (right) as in the middle panels except for the OGCM forced with twice-daily ECMWF winds.

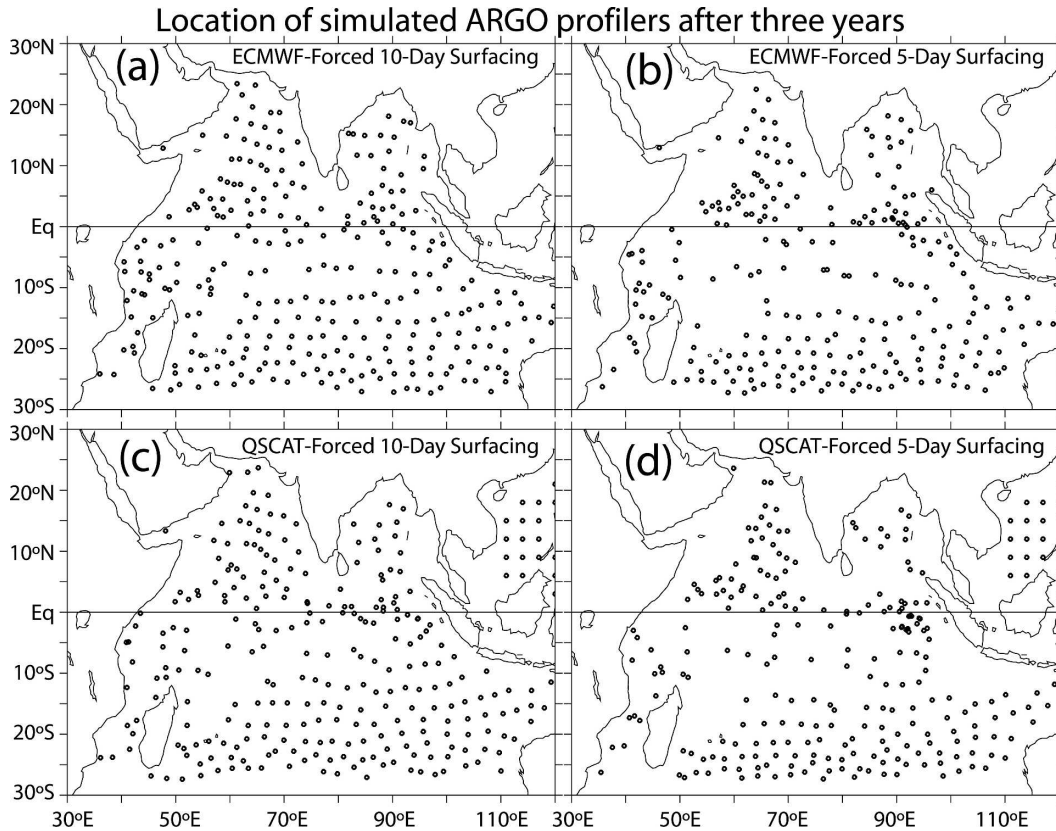


FIG. 5. Location of simulated Argo profiling floats 3 yr after deployment in a regular  $3^{\circ} \times 3^{\circ}$  array across the entire Indian Ocean: (a),(b) for the ECMWF-forced OGCM run and (c),(d) for the QuikSCAT-forced run.

years. The XBT lines considered in these experiments are shown in Fig. 1.

In our subsampling experiments we considered various repeat frequencies for the XBT lines, from weekly to semimonthly. Here we report on the results from two repeat frequencies: 1) “monthly” during which each frequently repeated XBT line is occupied on average 12 times a year and 2) “enhanced” for which XBT line IX-01 (Fremantle, Australia, to Sunda Strait, Indonesia) is repeated 52 times a year and all other lines 30 times a year. We find that the enhanced timing is fundamental for capturing the interannual variability in the heart of the Java and Somali upwelling zones and the southeastern Arabian Sea. We assume here that along each line the XBTs are dropped four times daily, that ship of opportunity travels at 20 kt, and that the ship track does not vary from that shown in the figure. The departure dates for the ships are assumed to vary by  $\pm 2$  days from a purely periodic series. For each virtual XBT profile (from 5 to 1000 m), the OGCM vertical temperature is interpolated to a regular 5-m grid; the actual XBT sampling rate is about once per meter, but that is much finer than any scale in the model.

### 3) MOORED BUOY ARRAY

An Indian Ocean mooring array is being deployed, and a configuration for it has been proposed and is shown in Fig. 1: this is the moored array explored in the OSSE experiments. The Autonomous Temperature Line Acquisition System (ATLAS) moorings currently deployed in the Indian Ocean have thermistors located at depths of 1 m (SST), 10, 20, 40, 60, 80, 100, 120, 140, 180, 300, and 500 m; we sample the OGCM daily mean temperature at each mooring location, linearly interpolated to each of these thermistor depths.

#### *b. Subsampled data gridding and analysis*

To explore the ability of the simulated observing system to resolve the seasonal to interannual variability of the Indian Ocean subsurface temperature, we place the subsampled data onto a regular grid through a two-step process. First, the subsampled OGCM data are binned to the Levitus grid, which has  $1^{\circ} \times 1^{\circ}$  horizontal resolution with 26 levels in the upper 2000 m. Twelve levels are in the top 300 m with spacing ranging from 10 m at the surface to 50 m between 150 and 300 m; spacing is

100 m between 400 and 1500 m, and 250 m below that. Binning is done at monthly time intervals. Subsampled OGCM data are equally weighted within each spatiotemporal region. Then, from the binned data, the number of observations and sample mean and variance are calculated. Various combinations of sensors are considered, ranging from single-component gridding (e.g., only Argo data included) to the complete observing system (i.e., Argo, XBT, and moorings all included).

To evaluate the seasonal to interannual variability of the subsampled data, more spatially complete datasets are generated from the initially sparse binned data by horizontal anomaly smoothing; anomalies are computed from the model monthly climatology. The anomaly smoothing procedure weights anomalies by the ratio of the standard deviation and the square root of the number of samples ( $\sigma/N^{1/2}$ ) and spreads the anomalies conservatively using a  $15^\circ$  zonal and  $7^\circ$  meridional cosine filter. More sophisticated analysis methods are both currently available and in development, but here we wish to evaluate the observing system rather than various analysis techniques and, thus, choose a simple and computationally inexpensive technique—one that allows us to evaluate multiple observing system configurations. We find that even with this relatively unsophisticated analysis technique the proposed IndOOS is able to capture the fundamental features of the interannual variability of the Indian Ocean.

### c. Subdaily variability

The tropical oceans (including the Indian Ocean) exhibit energetic variability on a broad range of time scales, including less than daily, which arises from the diurnal cycle, internal tides, turbulence, and other forms of variability. Moored buoys are able to sample relatively continuously (10-min sampling in the next-generation ATLAS and TRITON moorings), so variability on less than daily time scales is not significantly aliased into the moored observations. However, profiling observations, such as individual Argo samples and XBT profiles, are susceptible to aliasing of subdaily variability since they provide a snapshot in time of the vertical structure of the ocean at a point.

The model data used to perform the OSSE are saved as daily averages and the model does not have subdaily forcing applied to it, so the subdaily variability of the oceanic parameters must be parameterized. To estimate the subdaily temperature variability we examine the subdaily data that has been collected from the Tropical Atmosphere–Ocean (TAO) Array in the Pacific [Hayes et al. (1991) and McPhaden et al. (1998)] and the Pilot Research Moored Array in the Tropical Atlantic (PIRATA) in the Atlantic (Servain et al.

1998), as well as recently available data from two TRITON moorings in the Indian Ocean maintained by the Japan Marine Science and Technology Center (JAMSTEC). Ten-minute sampled subsurface temperature data for the TAO and PIRATA moorings are available, beginning in 1998 at the principal buoy locations, and can be downloaded from the NOAA/Pacific Marine Environmental Laboratory’s online data server (<http://pmel.noaa.gov/>); 10-min Indian Ocean TRITON data is available since late 2001 and made available by JAMSTEC.

There is considerable subdaily variability in temperature across the tropical Pacific and Atlantic Oceans and at the two Indian Ocean moorings; it is thus reasonable to expect it to be significant across the entire Indian Ocean. We compute the subdaily variation in temperature  $T'(t, z)$  at each buoy location as

$$T'(t, z) = T(t, z) - \langle T(t, z) \rangle,$$

where  $T(t, z)$  is the 10-min temperature at each thermistor depth ( $z$ ) and  $\langle T(t, z) \rangle$  is the 24-h-mean temperature centered at time  $t$ . Figures 6a and 6c show the profiles of the 1998–2004 standard deviation of the subdaily temperature variations  $\{\sigma_t[T'(t, z)]\}$  at each buoy location in the Pacific and Atlantic (lines are colored based on the longitude of the buoy); Fig. 6e shows the profile of  $\sigma_t[T'(t, z)]$  for each deployment of the two Indian Ocean TRITON moorings. Within the mixed layer and well below the thermocline,  $\sigma_t[T'(t, z)]$  is generally around  $0.1^\circ\text{C}$  at all locations, which suggests a simple parameterization at these depths as a normally distributed random number with standard deviation  $0.1^\circ\text{C}$ . However, near the thermocline,  $\sigma_t[T'(t, z)]$  exhibits much variation with depth at each location, and the  $\sigma_t(T'(t, z))$  varies significantly across each basin.

To compute a parameterization for  $T'(t, z)$  below the mixed layer, we assume that the subdaily temperature variations outside the mixed layer are driven adiabatically, principally through vertical advection acting on the background temperature gradient. We define a subdaily interface displacement  $[\eta'(t, z)]$  as

$$\eta'(t, z) = T'(t, z)(\partial/\partial z \langle T(t, z) \rangle)^{-1}.$$

Figures 6b, 6d, and 6f show profiles of the standard deviation of subdaily interface displacement  $\sigma_t[\eta'(t, z)]$ . Across the tropical Pacific Ocean,  $\sigma_t[\eta'(t, z)]$  exhibits a fairly consistent behavior near the thermocline, with an amplitude between 4 and 8 m. In the Atlantic Ocean, though there is more variability from location to location, the amplitude of  $\sigma_t[\eta'(t, z)]$  is between 4 and 10 m near the thermocline. The interface variability based on data from the two Indian Ocean mooring locations is

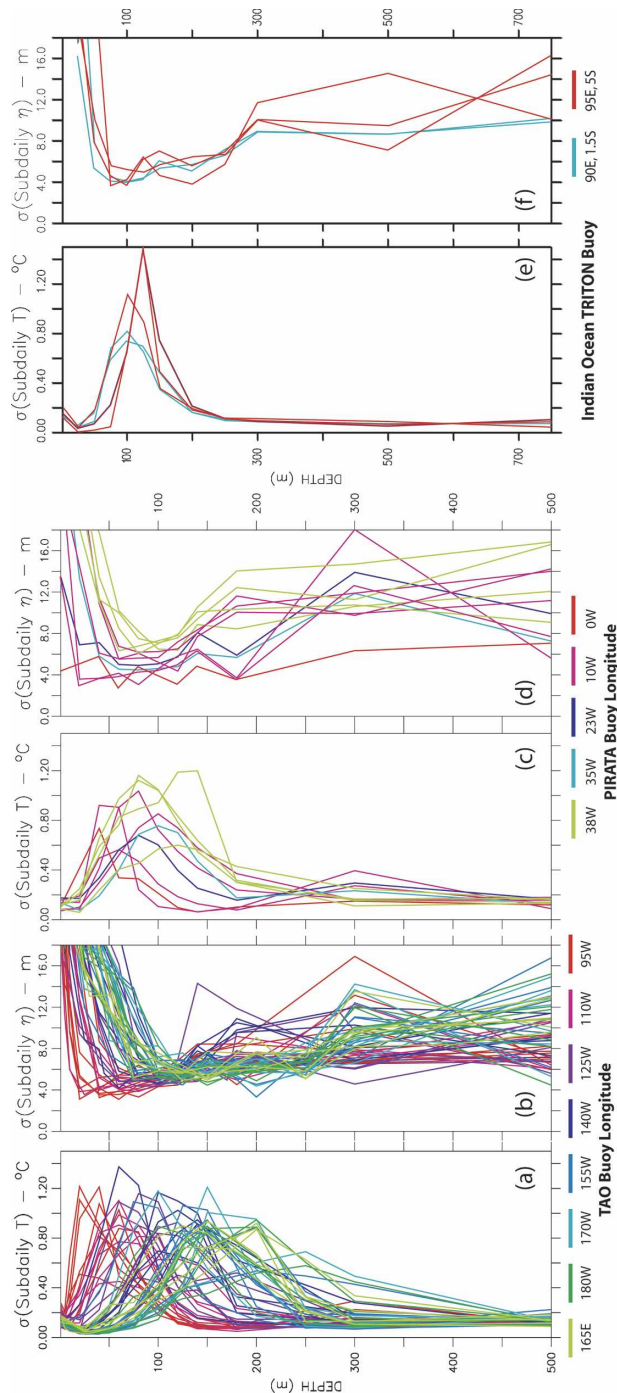


FIG. 6. Standard deviation of subdaily temperature for all (a) TAO-ATLAS, (c) PIRATA, and (e) Indian Ocean TRITON moorings, units:  $^{\circ}\text{C}$ . Standard deviation of estimated subdaily interface displacement for all (b) TAO-ATLAS, (d) PIRATA, and (f) Indian Ocean TRITON moorings, units: m. Values from TAO-ATLAS and PIRATA moorings computed over the period 1998–2004 and color coded based on model latitude. Values from the Indian Ocean TRITON moorings computed for each deployment and color coded by location.

consistent with that from the two other basins. In the OSSE experiments we will parameterize the subdaily variations near the thermocline as a product of the vertical temperature gradient and a normally distributed noise with a standard deviation of 7 m; in the mixed layer and well below the thermocline, a  $0.1^{\circ}\text{C}$  amplitude is used for the noise (the minimum amplitude of subdaily noise is  $0.1^{\circ}\text{C}$ ).

Because there are often multiple samples in a vertical averaging bin, an estimate of the vertical coherence of the subdaily noise is necessary. Multiple samples from the same profile will lead to a partial cancellation of the part of the noise that is not vertically coherent, but not to the noise that is vertically coherent. We computed the time correlation across vertically adjacent thermistors of the subdaily variability at the various moored buoy locations, and found that the correlation of thermistors within 10–20 m of each other was between 0.7 and 0.85. Thus, in constructing the subdaily temperature noise, we assume that half of the variance of subdaily vertical interface variations is incoherent with depth and half is vertically coherent ( $0.7^2 \approx 0.5$ ). Because our binning and analysis system treats each vertical level independently, we can simplify the distribution of the vertically coherent part of the noise by making it vertically uniform. To incorporate subdaily noise in an analysis system in which there is some explicit vertical coherence, further refinements need to be made to this formulation of the vertically coherent part of the noise.

It should be noted that dynamical models of the global oceanic internal tide have been developed (e.g., Arbic et al. 2004; Simmons et al. 2004), which could prove useful in future analyses of subdaily aliasing in observations. Further, high-frequency moored observations, like those described here, may be of use in tuning and evaluating these global tide models.

## 4. Results

### a. Interannual variability

The ability of different observing system configurations to capture the interannual variability of the subsurface temperature is explored in this section. We used the simple anomaly smoothing technique described in the previous subsection to generate basinwide datasets of the subsurface temperature anomaly for each observing system configuration and also performed an equivalent anomaly smoothing on the complete monthly mean data from the OGCM. To assess the observing system we have compared the root-mean-squared error (RMSE), correlation of monthly anomalies to the full dataset, and signal-to-noise ratio (defined

as the ratio of the standard deviation of the monthly anomaly from the fully resolved OGCM to the RMSE). We focus on the results from the 17-yr ECMWF-forced OGCM experiment since it is the one with the broadest representation of interannual variability (the QuikSCAT-forced run is only three years long).

We find that the fully integrated observing system provides a significantly improved sampling from that of any single observing system component, or pair of components. A fully deployed Argo profiling float array gives a useful description of the interannual subsurface temperature variability in most regions of the Indian Ocean. However, there are deficiencies in the equatorial regions and a degraded sampling near the coastal upwelling regions off Java/Sumatra and Somalia. As expected from the float drift maps shown in Fig. 5, the 5-day sampling strategy results in a degraded representation of the subsurface temperature variations, when compared to that from a 10-day sampling strategy. A moored buoy array spanning the region 15°S–10°N complements the deficiencies in the Argo sampling. The XBT lines provide important additional information across various regions, in particular the Somali, Arabian, and Java upwelling zones, and the southeast Arabian Sea. An XBT sampling more frequent than monthly is of particular impact in the upwelling zones, where other platforms are not able to do so suitably. These results are illustrated in Figs. 7–9.

Figure 7 shows the correlation of monthly mean 50-m temperature anomaly (generally within the oceanic mixed layer) from various sampling strategies and that from the OGCM; subsampled data are binned and smoothed as described in the previous subsection, and OGCM data is smoothed with a 15° zonal and 7° meridional filter to compare equivalent scales. Figure 7 (top left) indicates the standard deviation of the OGCM monthly 50-m temperature anomaly, showing areas of strong variability; the strongest variability is along the southern Indian Ocean thermocline ridge,

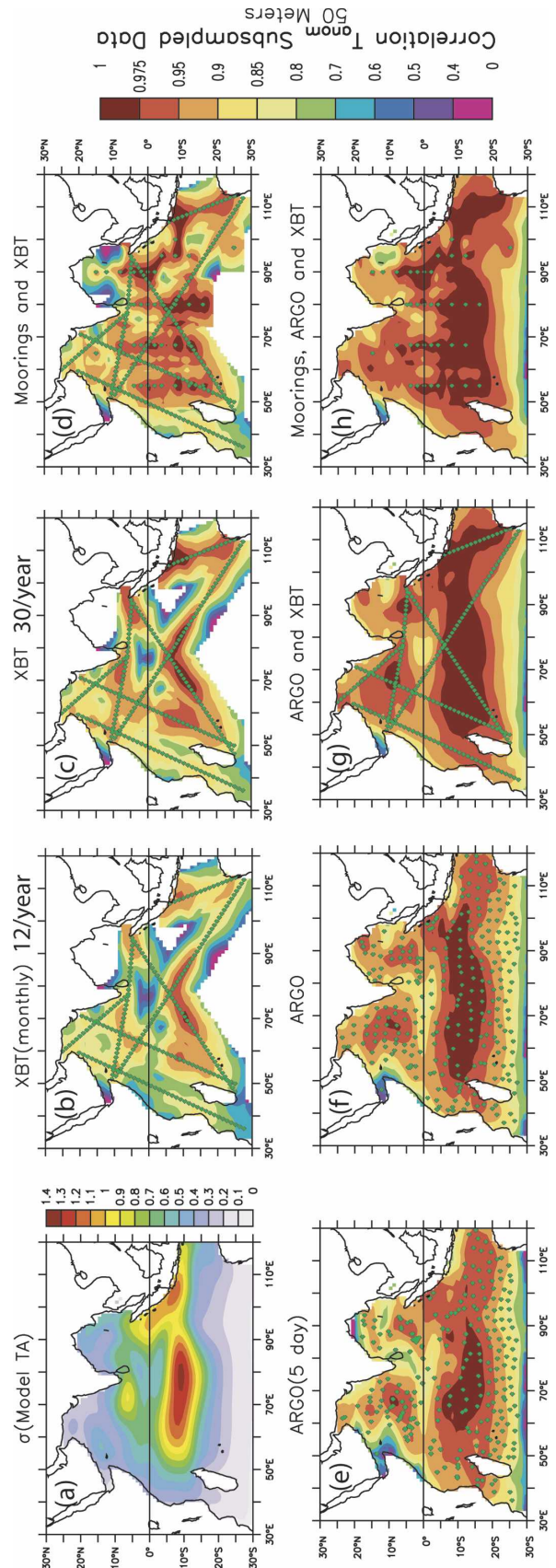


FIG. 7. Computed over the period 1986–2002: (a) standard deviation of monthly 50-m temperature anomaly from the ECMWF-forced OGCM, units: °C. Correlation of monthly 50-m temperature anomaly from the ECMWF-forced OGCM and that subsampled by (b) XBT lines done 12 times per year, (c) XBT lines performed 30 times per year except for IX-01 (52 times per year), (d) moored buoy array and 30 times per year XBTs, (e) 5-day interval Argo array, (f) 10-day interval Argo array, (g) 10-day interval Argo array and 30 times per year XBTs, and (h) Argo, moorings, and 30 times per year XBTs. Full OGCM data is smoothed with a 15° zonal and 7° meridional cosine filter; subsampled data are gridded and smoothed as described in section 3a.

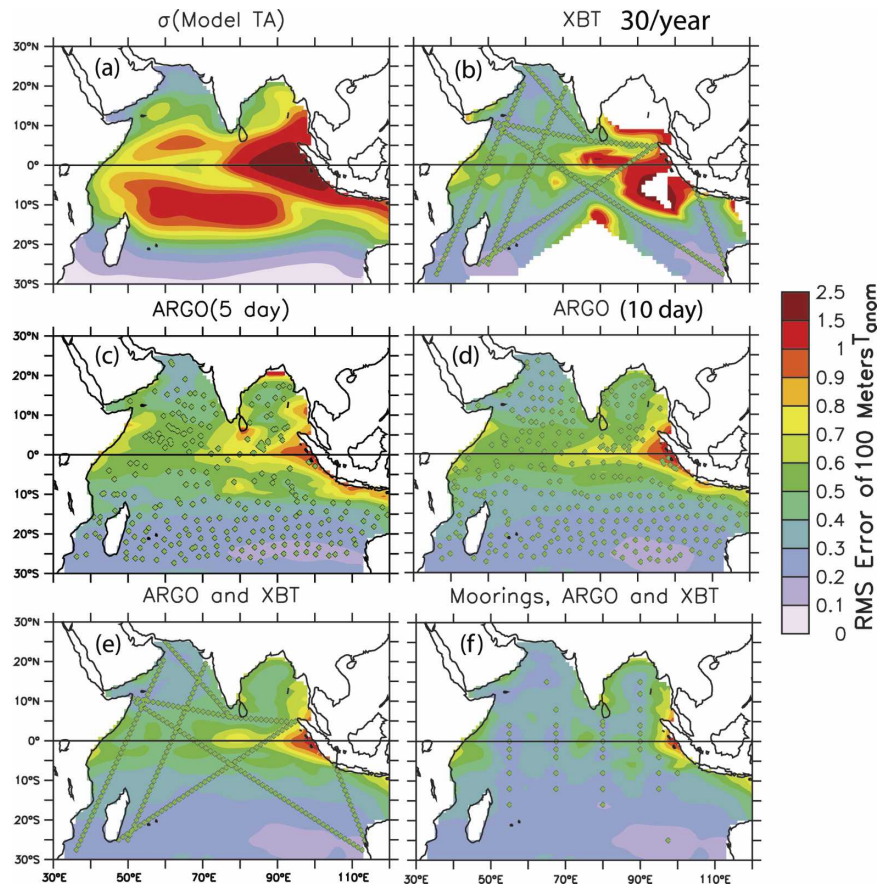


FIG. 8. Computed over the period 1986–2002: (a) standard deviation of the monthly 100-m temperature anomaly from the ECMWF-forced OGCM. Rms error of monthly 100-m temperature anomaly subsampled by (b) XBT lines performed 30 times per year except for IX-01 (52 times per year), (c) 5-day interval Argo array, (d) 10-day interval Argo array, (e) 10-day interval Argo array and 30 times per year XBTs, and (f) Argo, moorings, and 30 times per year XBTs. Units:  $^{\circ}\text{C}$ .

along the Java/Sumatra upwelling zone, and in the southeast Arabian Sea. There is also significant variability all along the equatorial waveguide, the eastern boundary of the Bay of Bengal, and the western Arabian Sea. Figure 7 (two middle-top panels) shows the correlation with two XBT sampling strategies; it is clear that much of the Indian Ocean is not adequately sampled by XBTs alone. XBT lines provide key information, however, along the coast of Java, the Somali upwelling zone, and the southeast Indian Ocean; they also provide sampling along the thermocline ridge. Addition of a moored buoy array to the XBT lines (Fig. 7, top right) improves the basinwide description of the interannual 50-m temperature variability—even with the unsophisticated analysis method used here.

The impact of an array of Argo profiling floats at two sampling intervals is shown in Fig. 7 (two leftmost lower panels). It is clear that the enhanced divergence of

Argo floats from regions of surface divergence seen in Fig. 5 results in a reduced effectiveness of sampling; the degradation of sampling is more evident from the 5-day sampling strategy. The addition of frequent XBT lines brings the correlations along the coast of Java above 0.975 and in the Somali upwelling zone above 0.9. The full observing system comprising a 10-day sampling Argo array, a moored buoy, and frequent XBT lines gives an extremely accurate description of the 50-m temperature anomaly field: correlations exceed 0.95 throughout much of the basin.

The impact of the different components is further highlighted in Fig. 8, which shows the rms error of monthly 100-m temperature anomalies (near or within the thermocline near the equator) from various observing system configurations. Figure 8 (top left), again, shows the standard deviation of the OGCM monthly 100-m temperature anomaly, indicating areas of strong

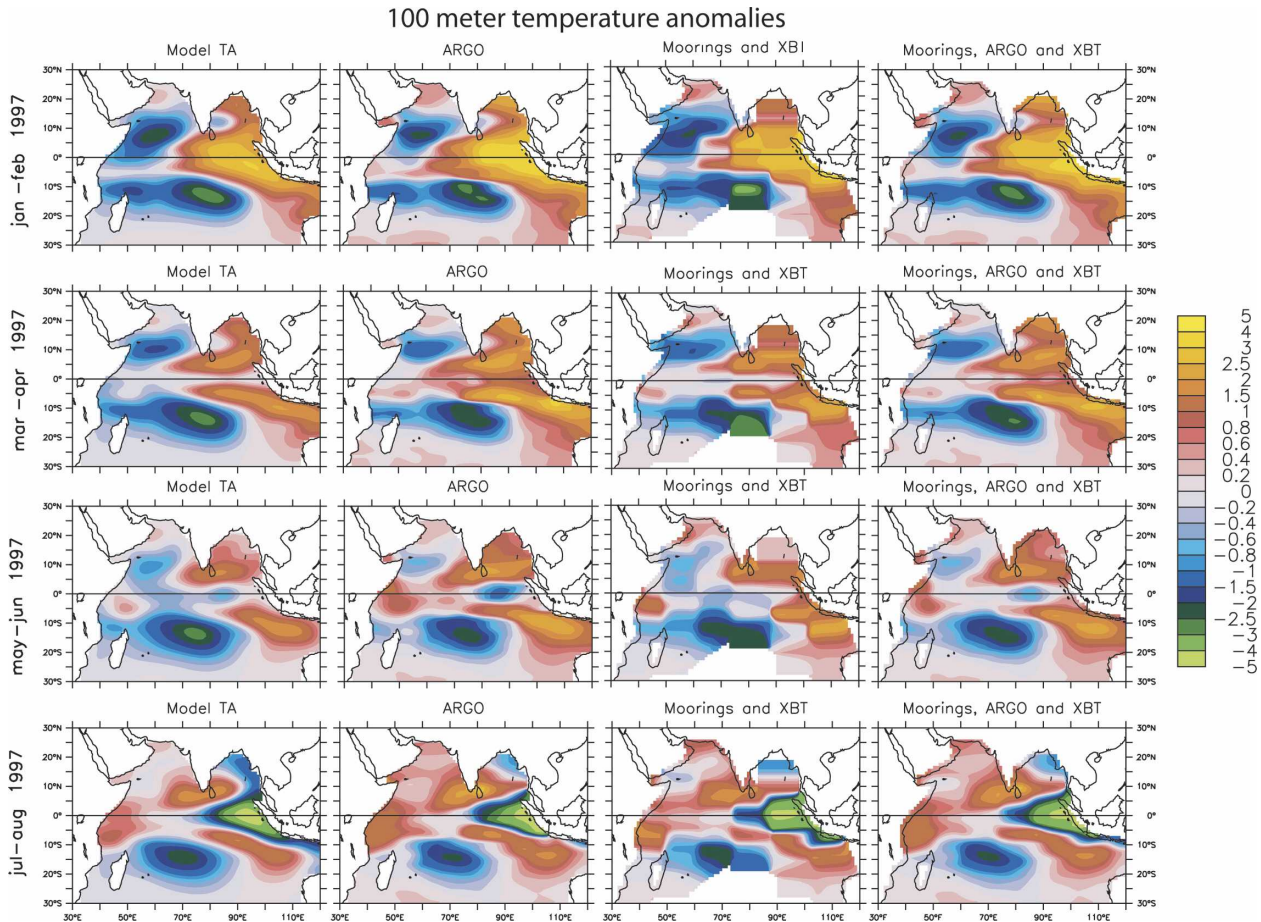


FIG. 9. Two-month-averaged 100-m temperature anomalies through the onset of the 1997–98 Indian Ocean dipole–zonal mode event as represented by (left column) the full OGCM; (second column) subsampled by the 10-day interval Argo array; (third column) subsampled by a moored buoy array and XBT lines performed 30 times per year except 52 times per year for IX-01; and (right column) subsampled by a full observing system consisting of the 10-day interval Argo array, moored buoy array, and XBT lines performed 30 times per year except 52 times per year for IX-01. Units: °C.

variability. The frequently repeated XBT lines result in rms errors generally between 0.5° and 1°C; the glaring exception is the eastern equatorial Indian Ocean, where rms errors exceed 1°C. This is a region of significant subseasonal variability, and its impact is seen in the data sampled by both Argo configurations and by the 10-day Argo+XBT configuration; without a moored array, the rms error of the monthly 100-m temperature anomaly equatorward of 10° exceeds 0.5°C. The inclusion of a moored buoy array into the 10-day sampling Argo array and the frequently repeated XBT lines brings the rms error over most of the Indian basin below 0.5°C. Figure 8 also shows the unintended degradation of Argo sampling resulting from attempting to resolve subseasonal variability by sampling at 5-day rather than 10-day intervals: the negative impact of sampling from the enhanced divergence of Argo floats

using a 5-day sampling can overwhelm the gains from increased time sampling.

The XBT results in Fig. 8, along with the subseasonal and subdaily temperature variability plots shown in Figs. 3 and 6, present a sobering reminder of potential impacts of the historical paucity of observations of subsurface temperature in many regions of the world—the Indian Ocean in particular. For example, assuming that the subseasonal and subdaily temperature variations are independent, in regions for which the observations from the two Indian Ocean TRITON moorings are representative, each instantaneous temperature measurement at the thermocline will have an rms error of  $\sim[(1.5^\circ\text{C})^2 + (1^\circ\text{C})^2]^{1/2}$ , or 1.8°C when used to estimate the seasonal-mean value. If we further assume that the subseasonal and subdaily variations are normally distributed, this implies that any individual observation of

temperature at the thermocline has a 50% chance of being more than  $1.2^{\circ}\text{C}$  away from the true monthly mean at the point.

The representation of the onset of the 1997–98 Indian Ocean dipole–zonal mode (IODZM) event using different observing system configurations gives insight into the ability of the observing system to resolve an important mode of variability. Figure 9 shows the 2-month mean 100-m temperature anomalies through the eight months preceding the onset of the 1997–98 IODZM from the OGCM (left column), an Argo array sampling at 10-day intervals (second column), a moored buoy array and frequent XBT lines (third column), and the full observing system (right column). Upon quick inspection, the evolution of the anomalies in all four columns is very similar: a pattern of cool SST in the west and warm SST in the east is slowly replaced by a warm west and cool east pattern. In fact, there are important differences in the anomalies resulting from sampling with Argo only (Fig. 9, second column) and those that include information from the moorings and XBTs. The differences occur principally along a narrow area confined to the equatorial waveguide and Java upwelling zone, but the dynamical interpretations of the observations are different.

A cold anomaly evident in the western equatorial Indian Ocean in January–February 1997 is well represented by the moorings/XBT, but is weak in the description from Argo. More noticeably in March–April and May–June 1997, there is a cold equatorial anomaly that grows beginning in the west and then becomes evident in the east (Fig. 9, second and third rows); this anomaly is well captured by the moorings. However, in the Argo representation, a cold anomaly in the eastern equatorial Indian Ocean appears to grow in place, surrounded by warm anomalies throughout. The interpretation of the evolution captured by the two observing systems is distinct: in that seen by Argo, local eastern Indian Ocean processes drove a local cold subsurface anomaly; in that seen by the moorings/XBT, the eastern Indian Ocean subsurface cooling was part of a basin-wide process. Finally, in July–August 1997, as the IODZM event is growing in the eastern Indian Ocean, the Argo representation of the anomalies misses the subsurface cooling off the coast of Java, which is well captured by a frequent XBT line from Fremantle to Sunda Strait (IX-01).

### *b. Subseasonal variability*

In this section we explore the ability of an observing system in the Indian Ocean to sample the energetic subseasonal variability of subsurface temperature. We

focus in particular on the improved representation of subseasonal variability resulting from 5-day rather than 10-day Argo sampling intervals. To compute the subseasonal temperature from the model and the Argo-sampled data, we first bin the data in  $10^{\circ}$  zonal,  $6^{\circ}$  meridional, and 10-day bins. The data are then averaged and a 60-day centered running mean is subtracted from the binned means. Figure 10 shows scatterplots of the 100-m subseasonal temperature anomalies from the OGCM (vertical axes) and from the Argo-sampled data (horizontal axes). Figure 10 (top row) shows the 10-day sampled data and the 5-day sampled data (bottom panel). Indicated in each panel are the correlation coefficients, the OGCM subseasonal standard deviation, and the root-mean-square error of the Argo-sampled data.

It is evident from Fig. 10 that both 10-day and 5-day Argo sampling is able to resolve aspects of the subseasonal equatorial 100-m temperature variability, though the signal-to-noise ratio is generally between 1 and 2. There is also a moderate improvement of the representation of the subseasonal variability by the 5-day sampling, over that from the 10-day sampling. At each location along the equator, the rms error decreases and the correlation values increase. However, the correlation increase is moderate, and the reduction in rms error is generally less than  $0.1^{\circ}\text{C}$ . We note that we chose to highlight the 100-m equatorial temperatures because they are in a region where the subseasonal signal is most energetic, and both the Argo representation and the improvement from 10-day to 5-day sampling is most favorable.

The moderate advantage of the 5-day sampling over the 10-day sampling in the ability of Argo to sample subseasonal variability evident in Fig. 10 is not a basin-wide feature and is confined principally to the equatorial thermocline. Even along the equator at 50 m (not shown), the improvement is unremarkable: in the bin centered at  $90^{\circ}\text{E}$  (where the largest improvement is evident), the rms error decreases from  $0.21^{\circ}$  to  $0.19^{\circ}\text{C}$ , and the correlation coefficient increases from 0.78 to 0.81. Thus, the gains in representation of subseasonal variability by the 5-day Argo sampling over the 10-day sampling are far from striking.

## **5. Summary and discussion**

We have presented an assessment of an integrated in situ Indian Ocean observing system (IndOOS) using a high-resolution ocean general circulation model (OGCM). We focused on the ability of an IndOOS comprising a  $3^{\circ} \times 3^{\circ}$  Argo profiling float array, a series

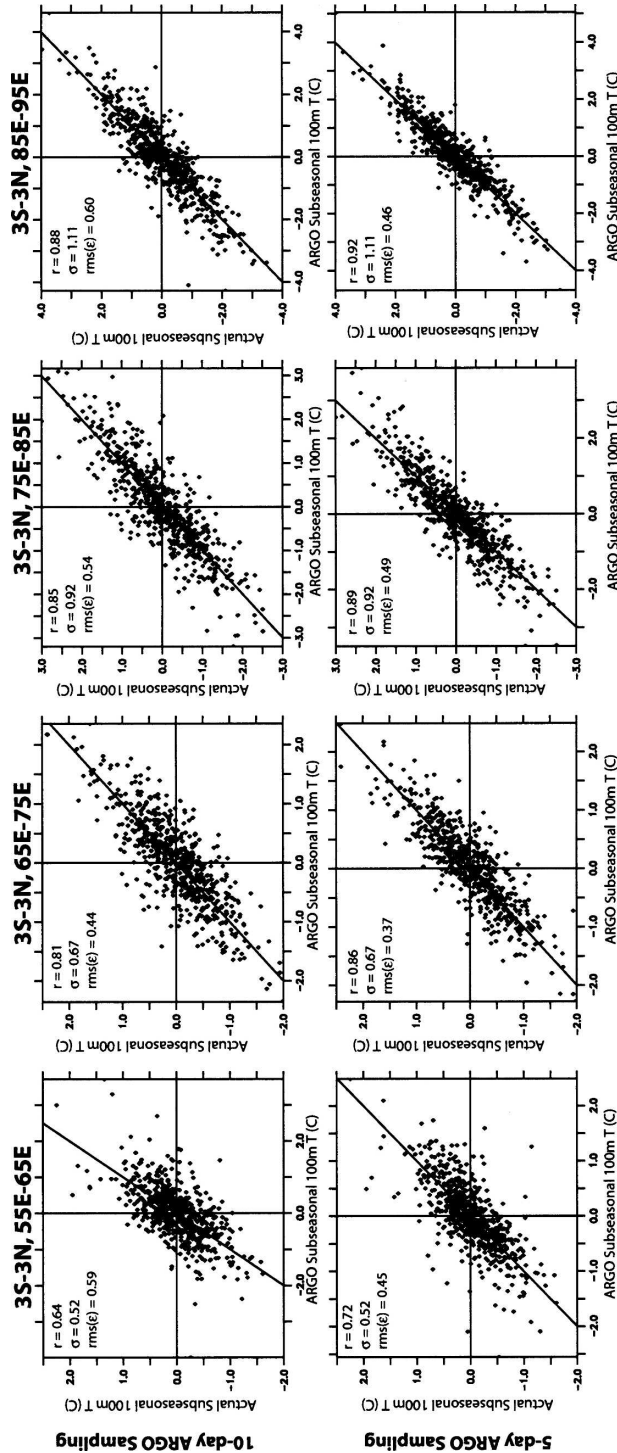


FIG. 10. Scatterplots of 50-m 10-day mean subsurface temperatures ( $<60$  day) from the full OGCM (vertical axes) and Argo-sampled OGCM (horizontal axes). (top) Values based on a 10-day sampling strategy, and (bottom) values based on a 5-day sampling strategy. Values computed by binning data in  $10^\circ$  zonal,  $6^\circ$  meridional, and 10-day bins. In each panel the correlation, standard deviation of the full OGCM data, and rms error of the subsampled data is indicated. Units:  $^\circ\text{C}$ .

of frequently repeated XBT lines, and an array of moored buoys (see CLIVAR–GOOS Indian Ocean Panel 2006) to observe the interannual and subseasonal variability of the subsurface Indian Ocean temperature. We developed an observationally based parameterization for subdaily noise, which was fundamental to our results; in the mixed layer it was parameterized as Gaussian noise with a rms of  $0.1^\circ\text{C}$ ; below the mixed layer, a Gaussian interface displacement with a standard deviation of 7 m is used (section 3c).

Interannual variability is captured well by the proposed system (section 4a). Argo gives a broad coverage with good sampling poleward of  $5^\circ$  and outside the Somali and Java/Sumatra coastal upwelling regions. Equatorward of  $5^\circ$ , moored buoys and XBT lines are essential, acting as complements to Argo in the observing system. The variability in the Somali and Java upwelling regions is sampled by XBT lines that should be run as frequently as possible; in particular, a weekly deployment of IX-01 (Fremantle to Sunda Strait) significantly enhances the resolution of variability off the Java upwelling region. We showed that the interpretation of the evolution of interannual changes in the equatorial waveguide can be obscured in the absence of moored buoys (section 4a; Fig. 9).

These OSSE experiments indicate that even when sampling at 5-day intervals, Argo does not significantly improve the representation of subseasonal variability in the Indian Ocean (section 4b): the amplitude of the subseasonal variability is of the same order as that of the subdaily temperature noise, the spatial scales of the intraseasonal signal are relatively short, and much of the Indian Ocean intraseasonal variability occurs on submonthly time scales (e.g., Sengupta and Ravichandran 2001; Harrison and Vecchi 2001; Vecchi and Harrison 2002; Sengupta et al. 2004; Masumoto et al. 2005a). Our findings differ from those of Schiller et al. (2004); the difference can likely be attributed to our inclusion and parameterization of subdaily variability in our OSSE, the higher spatial resolution of our OGCM ( $0.33^\circ\text{--}0.5^\circ \times 0.33^\circ$  versus  $2^\circ \times 0.5^\circ\text{--}1.5^\circ$ ), and our use of daily, rather than 3 day, wind forcing and model output.

Because practically all of the horizontal displacement of simulated Argo floats occurred while they were at the surface, halving the sampling interval (from 10 to 5 days) of the simulated Argo floats doubles the rate at which floats move away from regions of surface current divergence and increases the spatial aliasing by the floats. The OGCM experiments suggest that there is negligible added value to a 5-day sampling strategy, and significant potential disadvantage, thus arguing for the

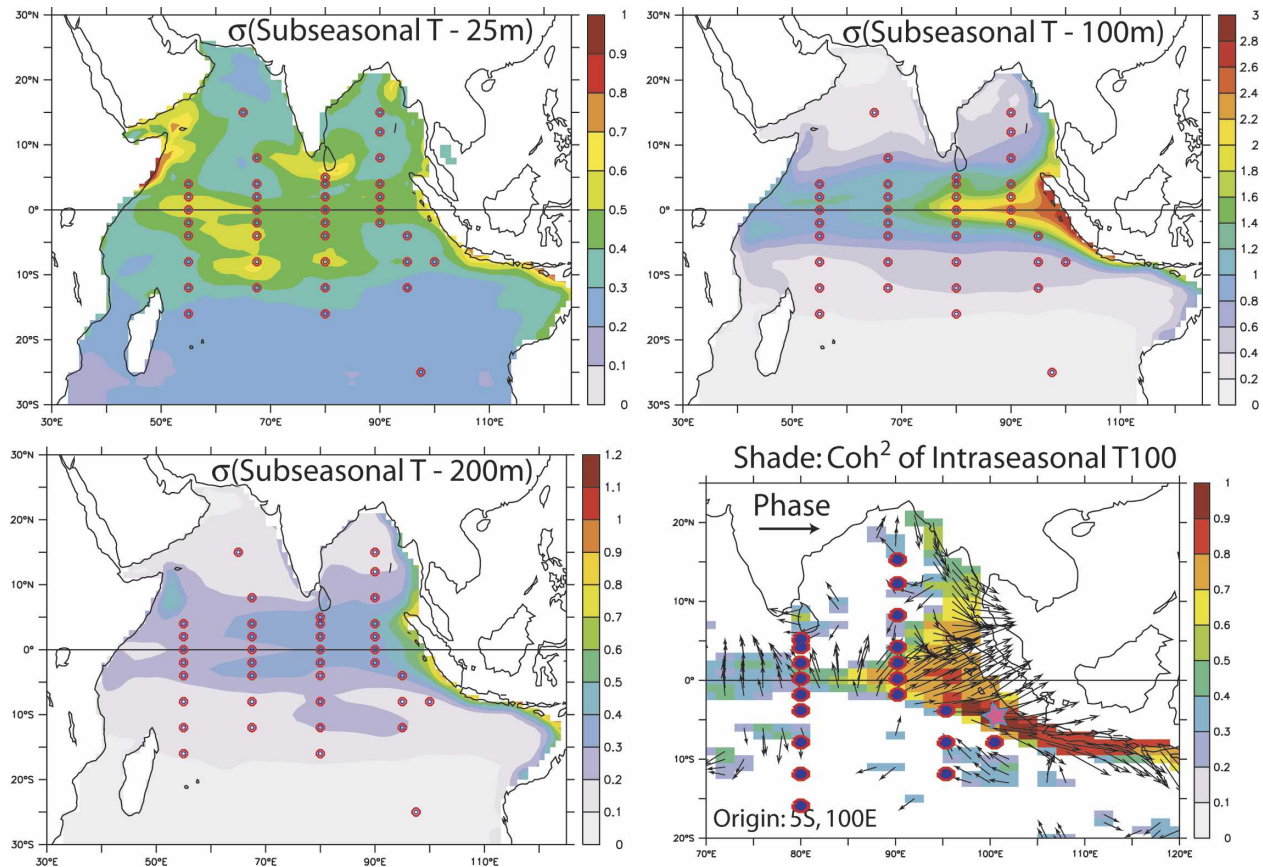


FIG. 11. Standard deviation of subseasonal (<61 day) temperature from the intraseasonally enhanced OGCM (see section 2) at (a) 25 m, (b) 100 m, and (c) 200 m. Shown in (a)–(c) are the locations of the proposed moorings. (d) The 90% significant coherence squared values of subseasonal (15–41 day) 100-m temperature anomalies; vectors indicate the phase angle (due east is 0°, due north is leading by 90°) referenced to 5°S, 100°E.

standard 10-day sampling to be adopted throughout the basin. This result illustrates one of the potential pitfalls in designing an OSSE based on optimization: in complex systems optimization of a particular cost function can result in the unintended degradation of other features. The multimodel, multistrategy efforts that have been pursued thus far in the Indian Ocean have allowed the parties coordinating and deploying the observing system to weigh the results from various groups (e.g., Schiller et al. 2004; Oke and Schiller 2007; Ballabrera-Poy et al. 2007; T. Lee 2005, personal communication).

Because of continuous time sampling, a moored buoy array does not need to contend with temporal aliasing in its representation of the subseasonal variability. In fact, the simulated mooring array in these OSSE experiments is able to resolve much of the subseasonal variability in the OGCM. A mooring array spanning the equator, thermocline ridge, and Bay of Bengal is an essential component of any observing system seeking to capture the energetic and socially relevant subseasonal

variability in the Indian Ocean. The proposed mooring array shown in Fig. 1 spans most of the regions of energetic subseasonal variability in the OGCM (Fig. 11). However, notable exceptions are the upwelling regions off the coast of Somalia and Java/Sumatra; both of these regions are of significant climate interest (e.g., Saji et al. 1999; Webster et al. 1999; Vecchi and Harrison 2004; Vecchi et al. 2004). Because of their proximity to land and the active fisheries present in those regions, expected losses to vandalism and snares with fishing equipment make mooring deployment in these regions unfeasible; the utility of developing observational technologies, such as autonomous gliders (e.g., Eriksen et al. 2001; Sibenac et al. 2004), to sample directly in these regions should be explored. However, the subsurface subseasonal variability along the coast of Java/Sumatra (e.g., 5°S, 100°E) exhibits strong coherence with variability along the equatorial waveguide, at the location of the proposed moorings (Fig. 11d). It is possible that information from the moorings along the waveguide

and near Java/Sumatra could be used to describe the variability along the coastal waveguide.

The anomaly smoothing procedure produces a reasonable analysis, despite ad hoc assumptions about the correlation scales and the errors. More sophisticated techniques, such as a model-based assimilation would be expected to produce a higher quality analysis. For instance, propagation of anomalies along the equatorial waveguide and the coast of Java/Sumatra is absent from our analysis procedure. Furthermore, information from satellite altimetry is not incorporated in our analysis. Future work should be directed toward comparing our results to such data assimilation products.

The OSSE experiments described here show that an integrated observing system in the Indian Ocean comprised of frequently repeated XBT lines, a  $3^{\circ} \times 3^{\circ}$  Argo profiling float array sampling at 10-day intervals, and a moored buoy array is able to resolve the principal characteristics of interannual and subseasonal subsurface temperature variability in the Indian Ocean. Even with an unsophisticated data analysis technique, we are able to reproduce the variability in an OGCM subsampled as the observing system would do. Fundamental to our ability to perform the OSSEs were the existence of observations with which to calibrate the model: moored observations allowed for the correction of an underenergetic model subseasonal variability and for the development of a parameterization of subdaily temperature variability. As the observing system is deployed, our understanding and awareness of modes of variability in the Indian Ocean will grow, and future ocean-only and coupled-model simulations of the Indian Ocean will likely improve due to them.

*Acknowledgments.* This research was supported by the Visiting Scientist Program at the National Oceanic and Atmospheric Administration's Geophysical Fluid Dynamics Laboratory (NOAA/GFDL), administered by the University Corporation for Atmospheric Research (UCAR). Analysis and graphics were done using the freeware package Ferret (information available online at <http://ferret.pmel.noaa.gov/>). We acknowledge the TAO project office for making the TAO and PIRATA buoy data easily and readily available; we are grateful to Drs. Yukio Masumoto and Yoshi Kuroda for kindly making the high-frequency Indian Ocean TRITON data available. Helpful comments and suggestions were received from the CLIVAR Indian Ocean Panel, Ed Harrison, Scott Song, Tony Rosati, Andrew Wittenberg, Bob Hallberg, Brian Arbic, and Sebastian Ilcane. We acknowledge the careful reading by and useful suggestions from the three anonymous reviewers.

## REFERENCES

- Annamalai, H., and R. Murtugudde, 2004: Role of the Indian Ocean in regional climate variability. *Earth Climate: The Ocean-Atmosphere Interaction, Geophys. Monogr.*, Vol. 147, Amer. Geophys. Union, 213–246.
- Arbic, B. K., S. T. Garner, R. W. Hallberg, and H. L. Simmons, 2004: The accuracy of surface elevations in forward global barotropic and baroclinic tide models. *Deep-Sea Res. II*, **51**, 3069–3101.
- Argo Science Team, 2001: The global array of profiling floats. *Observing the Oceans in the 21st Century*, C. J. Koblinsky and N. R. Smith, Eds., GODAE Project Office, 248–258.
- Ballabrera-Poy, J., E. Hackert, R. Murtugudde, and A. J. Busalacchi, 2007: An observing system simulation experiment for an optimal moored instrument array in the tropical Indian Ocean. *J. Climate*, **20**, 3284–3299.
- Bhat, G. S., and Coauthors, 2001: BOBMEX: The Bay of Bengal Monsoon Experiment. *Bull. Amer. Meteor. Soc.*, **82**, 2217–2243.
- , G. A. Vecchi, and S. Gadgil, 2004: Sea surface temperature of the Bay of Bengal derived from TRMM. *J. Atmos. Oceanic Technol.*, **21**, 1283–1290.
- Bond, N. A., and G. A. Vecchi, 2003: On the Madden-Julian oscillation and precipitation in Oregon and Washington. *Wea. Forecasting*, **18**, 600–613.
- Boyer, T. F., S. Levitus, J. L. Antonov, R. A. Locarnini, and H. E. Garcia, 2005: Linear trends in salinity of the World Oceans, 1955–1998. *Geophys. Res. Lett.*, **32**, L01604, doi:10.1029/2004GL021791.
- CLIVAR-GOOS Indian Ocean Panel, 2006: Understanding the role of the Indian Ocean in the climate system—Implementation plan for sustained observations. WCRP Informal Rep. 5/2006, ICPO Publications Series 100, GOOS Rep. 152, 78 pp.
- Duvel, J. P., R. Roca, and J. Vialard, 2004: Ocean mixed layer temperature variations induced by intraseasonal convective perturbations over the Indian Ocean. *J. Atmos. Sci.*, **61**, 1004–1023.
- ECMWF, 1989: The description of the ECMWF/WCRP level III—A global atmospheric data archive. ECMWF Tech. Attachment, 72 pp. [Available from ECMWF, Shinfield Park, Reading RG2 9AX, United Kingdom.]
- Eriksen, C. C., T. J. Osse, R. D. Light, T. Wen, T. W. Lehman, P. L. Sabin, J. W. Ballard, and A. M. Chiodi, 2001: Seaglider: A long-range autonomous underwater vehicle for oceanographic research. *IEEE J. Oceanic Eng.*, **26**, 424–436.
- Fu, X., B. Wang, T. Li, and J. McCreary, 2003: Coupling between northward propagating, intraseasonal oscillations and sea surface temperature in the Indian Ocean. *J. Atmos. Sci.*, **60**, 1733–1753.
- Gualdi, S., E. Guilyardi, A. Navarra, S. Masina, and P. Delecluse, 2003: The interannual variability in the Indian Ocean as simulated by a CGCM. *Climate Dyn.*, **20**, 567–582.
- Harrison, D. E., 1989: On climatological monthly mean wind stress and wind stress curl fields over the World Ocean. *J. Climate*, **2**, 57–70.
- , and N. K. Larkin, 1998: The COADS sea level pressure signal: A near-global El Niño composite and time series view, 1946–1993. *J. Climate*, **9**, 3025–3055.
- , and G. A. Vecchi, 2001: January 1999 Indian Ocean cooling event. *Geophys. Res. Lett.*, **28**, 3717–3720.
- Hayes, S. P., L. J. Mangum, J. Picaut, A. Sumi, and K. Takeuchi, 1991: TOGA-TAO: A moored array for real-time measure-

- ments of the tropical Pacific Ocean. *Bull. Amer. Meteor. Soc.*, **72**, 339–347.
- Ju, J., and J. M. Slingo, 1995: The Asian summer monsoon and ENSO. *Quart. J. Roy. Meteor. Soc.*, **121**, 1133–1168.
- Kummerow, C., and Coauthors, 2000: The status of the Tropical Rainfall Measuring Mission (TRMM) after two years in orbit. *J. Appl. Meteor.*, **39**, 1965–1982.
- Large, W. G., and S. Pond, 1981: Open-ocean momentum-flux measurements in moderate to strong winds. *J. Phys. Oceanogr.*, **11**, 324–336.
- , and —, 1982: Sensible and latent heat-flux measurements over the ocean. *J. Phys. Oceanogr.*, **12**, 464–482.
- Larkin, N. K., and D. E. Harrison, 2001: Tropical Pacific ENSO cold events, 1946–95: SST, SLP, and surface wind composite anomalies. *J. Climate*, **14**, 3904–3931.
- Lau, N. C., and M. J. Nath, 2003: Atmosphere–ocean variations in the Indo–Pacific sector during ENSO episodes. *J. Climate*, **16**, 3–20.
- Levitus, S., 1982: *Climatological Atlas of the World Ocean*. NOAA Prof. Paper 13, 173 pp. and 17 microfiche.
- , J. Antonov, and T. Boyer, 2005: Warming of the world ocean, 1955–2003. *Geophys. Res. Lett.*, **32**, L02604, doi:10.1029/2004GL021592.
- Loshnigg, J., and P. J. Webster, 2000: A coupled ocean–atmosphere system of SST modulation for the Indian Ocean. *J. Climate*, **13**, 3342–3360.
- Madden, R. A., and P. R. Julian, 1994: Observations of the 40–50-day tropical oscillation: A review. *Mon. Wea. Rev.*, **122**, 814–837.
- Maloney, E. D., and D. L. Hartmann, 2000: Modulation of eastern North Pacific hurricane activity in the Gulf of Mexico by the Madden–Julian oscillation. *Science*, **287**, 2002–2004.
- Mariano, A. J., E. H. Ryan, B. D. Perkins, and S. Smithers, 1995: The Mariano global surface velocity analysis 1.0. Tech. Rep. CG-D-34-95, Office of Engineering, Logistics, and Development, U.S. Coast Guard, 55 pp.
- Masumoto, Y., H. Hase, Y. Kuroda, H. Matsuura, and K. Takeuchi, 2005a: Intraseasonal variability in the upper layer currents observed in the eastern equatorial Indian Ocean. *Geophys. Res. Lett.*, **32**, L02607, doi:10.1029/2004GL021896.
- , V. S. N. Murty, M. Jury, M. J. McPhaden, P. Hacker, J. Vialard, R. Molcard, and G. Meyers, cited 2005b: Tropical Indian Ocean mooring array: Present status and future plans. [Available online at [http://ioc.unesco.org/oopc/oopc9/Tropical\\_Indian\\_Moorings.pdf](http://ioc.unesco.org/oopc/oopc9/Tropical_Indian_Moorings.pdf).]
- McPhaden, M. J., and Coauthors, 1998: The Tropical Ocean–Global Atmosphere (TOGA) observing system: A decade of progress. *J. Geophys. Res.*, **103**, 14 169–14 240.
- Meyers, G., and Coauthors, 2000: Monsoon, seasonal and interannual applications of an Indian Ocean observing system. *Observing the Ocean in the 21st Century*, C. J. Koblinsky and N. R. Smith, Eds., Bureau of Meteorology, 48–65.
- Miyama, T., J. P. McCreary, T. G. Jensen, J. Loschnigg, S. Godfrey, and A. Ishida, 2003: Structure and dynamics of the Indian Ocean cross-equatorial cell. *Deep-Sea Res. II*, **50**, 2023–2047.
- Mo, K. C., and R. W. Higgins, 1998: Tropical convection and precipitation regimes in the western United States. *J. Climate*, **11**, 2404–2423.
- Nicholls, N., 1995: All-India summer monsoon rainfall and sea surface temperature around northern Australia and Indonesia. *J. Climate*, **8**, 1463–1467.
- Oke, P. R., and A. Schiller, 2007: A model-based assessment and design of a tropical Indian Ocean mooring array. *J. Climate*, **20**, 3269–3283.
- Pacanowski, R. C., and S. G. H. Philander, 1981: Parametrizations of vertical mixing in numerical models of tropical oceans. *J. Phys. Oceanogr.*, **11**, 1443–1451.
- Premkumar, K., M. Ravichandran, S. R. Kalsi, D. Sengupta, and S. Gadgil, 2000: First results from a new observational system over the Indian seas. *Curr. Sci.*, **78**, 323–330.
- Reynolds, R. W., and T. M. Smith, 1994: Improved global sea surface temperature analyses using optimum interpolation. *J. Climate*, **7**, 929–948.
- , N. A. Rayner, T. M. Smith, D. C. Stokes, and W. Wang, 2002: An improved in situ and satellite SST analysis for climate. *J. Climate*, **15**, 1609–1625.
- Richardson, P. L., and T. K. McKee, 1989: Surface velocity in the equatorial oceans (20N–20S) calculated from historical ship drifts. WHOI Tech. Rep. WHOI-89-9, Woods Hole Oceanographic Institution, Woods Hole, MA, 50 pp.
- Saji, N. H., B. N. Goswami, P. N. Vinayachandran, and T. Yamagata, 1999: A dipole mode in the tropical Indian Ocean. *Nature*, **401**, 360–363.
- Schiller, A., S. E. Wijffels, and G. A. Meyers, 2004: Design requirements for an Argo float array in the Indian Ocean inferred from observing system simulation experiments. *J. Atmos. Oceanic Technol.*, **21**, 1598–1620.
- Schott, F. A., and J. P. McCreary, 2001: The monsoon circulation of the Indian Ocean. *Prog. Oceanogr.*, **51**, 1–123.
- , —, and G. C. Johnson, 2004: Shallow overturning circulations of the tropical–subtropical oceans. *Earth Climate: The Ocean–Atmosphere Interaction*, *Geophys. Monogr.*, Vol. 147, Amer. Geophys. Union, 261–304.
- Sengupta, D., and M. Ravichandran, 2001: Oscillations of Bay of Bengal sea surface temperature during the 1998 summer monsoon. *Geophys. Res. Lett.*, **28**, 2033–2036.
- , R. Senan, V. S. N. Murty, and V. Fernando, 2004: A bi-weekly mode in the equatorial Indian Ocean. *J. Geophys. Res.*, **109**, C10003, doi:10.1029/2004JC002329.
- Servain, J., A. J. Busalacchi, M. J. McPhaden, A. D. Moura, G. Reverdin, M. Vianna, and S. E. Zebiak, 1998: A Pilot Research Moored Array in the Tropical Atlantic (PIRATA). *Bull. Amer. Meteor. Soc.*, **79**, 2019–2031.
- Sibenac, M., T. Podder, W. Kirkwood, and H. Thomas, 2004: Autonomous underwater vehicles for ocean research: Current needs and state of the art technologies. *Mar. Technol. Soc. J.*, **38** (2), 63–72.
- Simmons, H. L., R. W. Hallberg, and B. K. Arbic, 2004: Internal wave generation in a global baroclinic tide model. *Deep-Sea Res. II*, **51**, 3043–3068.
- Smith, W. H. F., and D. T. Sandwell, 1997: Global sea floor topography from satellite altimetry and ship depth soundings. *Science*, **277**, 1956–1962.
- Song, Q. N., G. A. Vecchi, and A. Rosati, 2007: Indian Ocean variability in the GFDL coupled climate model. *J. Climate*, **20**, 2895–2916.
- Vecchi, G. A., and D. E. Harrison, 2002: Monsoon breaks and subseasonal sea surface temperature variability in the Bay of Bengal. *J. Climate*, **15**, 1485–1493.
- , and —, 2003: On the termination of the 2002–03 El Niño event. *Geophys. Res. Lett.*, **30**, 1964, doi:10.1029/2003GL017564.
- , and N. A. Bond, 2004: The Madden–Julian Oscillation (MJO) and northern high latitude wintertime surface air tem-

- peratures. *Geophys. Res. Lett.*, **31**, L04104, doi:10.1029/2003GL018645.
- , and D. E. Harrison, 2004: Interannual Indian rainfall variability and Indian Ocean sea surface temperature anomalies. *Earth Climate: The Ocean–Atmosphere Interaction, Geophys. Monogr.*, Vol. 147, Amer. Geophys. Union, 247–260.
- , and —, 2005: The termination of the 1997–98 El Niño. Part I: Mechanisms of oceanic change. *J. Climate*, **19**, 2633–2646.
- , S.-P. Xie, and A. Fischer, 2004: Air–sea coupling over western Arabian Sea cold filaments. *J. Climate*, **17**, 1213–1224.
- Wang, B., P. J. Webster, and H. Teng, 2005: Antecedents and self-induction of active-break south Asian monsoon unraveled by satellites. *Geophys. Res. Lett.*, **32**, L04704, doi:10.1029/2004GL020996.
- Webster, P. J., V. O. Magana, T. N. Palmer, J. Shukla, R. A. Tomas, M. Yanai, and T. Yasunari, 1998: Monsoons: Processes, predictability and prospects for prediction. *J. Geophys. Res.*, **103**, 14 451–14 510.
- , A. M. Moore, J. P. Loschnigg, and R. R. Leben, 1999: Coupled ocean–atmosphere dynamics in the Indian Ocean during 1997–98. *Nature*, **401**, 356–360.
- , and Coauthors, 2002: The JASMINE pilot study. *Bull. Amer. Meteor. Soc.*, **83**, 1603–1630.
- Xie, S. P., H. Annamalai, F. A. Schott, and J. P. McCreary, 2002: Structure and mechanisms of South Indian Ocean climate variability. *J. Climate*, **15**, 864–878.
- Yamagata, T., S. K. Behera, J.-J. Luo, S. Masson, M. R. Jury, and S. A. Rao, 2004: Coupled ocean–atmosphere variability in the tropical Indian Ocean. *Earth Climate: The Ocean–Atmosphere Interaction, Geophys. Monogr.*, Vol. 147, Amer. Geophys. Union, 189–211.